Electronic supplementary information for

Non-covalent interactions in ionic liquid ion pairs and ion pair dimers: A quantum chemical calculation analysis

Bogdan A. Marekha, Oleg N. Kalugin, and Abdenacer Idrissi

Level of theory validation: $MmimBF_4$ model system

Dispersion plays significant role in ILs and, hence, acquiring reliable results from computational studies requires a good enough level of theory to capture such effects.[1-4] Hydrogen bonding in ILs also remains a rather open question and special care needs to be taken in theoretical calculations as well as in the interpretation of experimental results.[5] At present, the highest employed level of theory for geometry optimizations of imidazolium IL ion pairs is MP2/aug-cc-pVTZ[6, 7] and MP2/aug-cc-pVDZ for larger aggregates.[7] Single point energy estimations were feasible even with CCSD(T)/complete basis set extrapolation.[8] However, these front-end calculation studies already require enormous amount of time and memory resources on modern supercomputers for model systems containing a small 1,3-dimethylimidazolium ($Mmim^+$) cation and/or monoatomic anion. This is definitely unaffordable for routine studies where it is not the ultrahigh precision, particularly in the energy values, which is needed, but rather reliable geometries and other properties, which capture all the key peculiarities of a given system.

In order to select a reasonable level of theory for our calculations, we performed a small benchmark study on $MmimBF_4$ ion pair in vacuum (see Fig. ESI1.). This model ion pair was selected as the smallest one to have the main features of our systems of interest, namely, a dialkylimidazolium cation and a multiatomic perfluorinated anion. In the optimized geometry, anion is located symmetrically on top of the C^2-H^2 fragment, which is the most positively charged one in the dialkylimidazolium cations,[9] and establishes a number of short non-covalent contacts between its fluorine atoms and the C^2-H^2 fragment as well as with the adjacent alkyl groups.

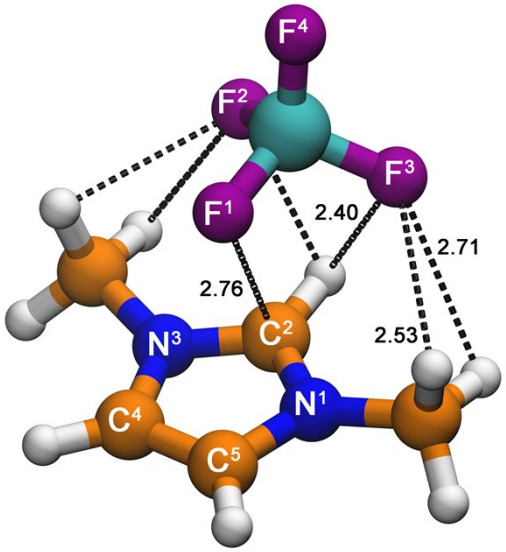

Fig. ESI1. Optmized geometry of $MmimBF_4$ ion pair obtained at MP2/6-311++g(d,p) level of theory. Key interionic short contacts are indicated with dashed black lines. Symmetry unique distances are given in Å. Color coding of the elements: white – H, orange – C, blue – N, purple – F, cyan – B.

The optimal geometries, which are used to define the interaction energies, electron density distribution and other derived properties of interest, obtained with the different methods are compared in Fig. ESI2. We note that the common B3LYP method with the basis set 6-31+g(d) erroneously predicts the anion to be asymmetrically tilted and positioned more towards the in-plane orientation, *i.e.*, more in front of the C^2-H^2 fragment, rather than on top of it (Fig. ESI2 *B*). Moreover, a larger basis set 6-311++g(d,p) does not fix the problem, and neither do the B97D and wB97xD functionals. They only shift the anion closer to the on-top of the C^2-H^2 fragment, but it is still asymmetrically tilted. It is only with the B3LYP-D3 method that we could obtain a symmetrical structure compatible with the reference one. We stress that this is an inherent problem of these functionals and not due to a bad choice of the initial configuration: It was impossible for us to remain in a symmetric structure with the B3LYP, B97D, and wB97xD functionals even when the MP2 structure was used as the starting one and very strict convergence thresholds were employed.

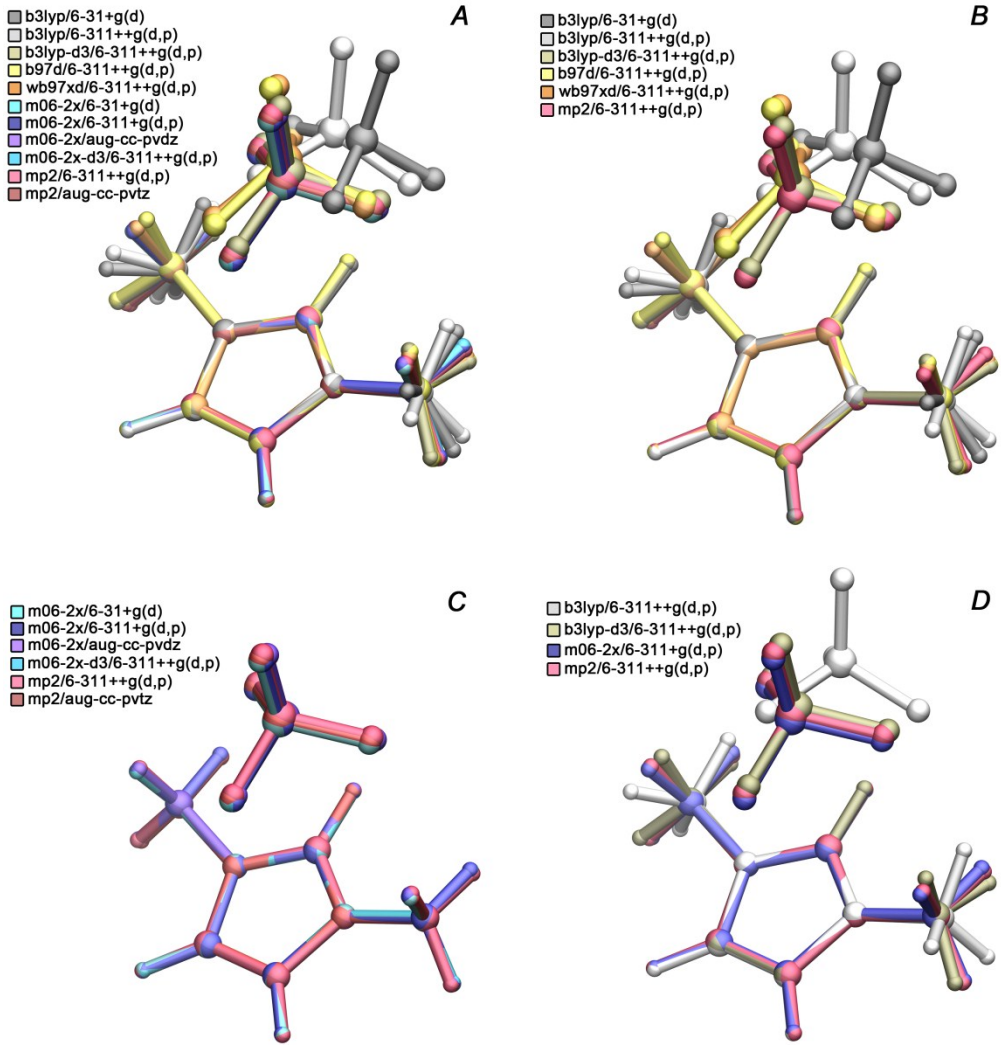

Fig. ESI2. Overlayed by the imidazolium ring optimized in vacuum structures of MmimBF$_4$ ion pair as obtained at different levels of theory. A – overall comparison of all the tested approaches. B – assessment of the DFT-D2/D3 style correction. C – assessment of the basis set dependence for the M06-2X functional. D – comparison of B3LYP, B3LYP-D3, and M06-2X functionals coupled with the 6-311++g(d,p) basis set. The reference structure obtained at the MP2/6-311++g(d,p) level of theory is shown in all the panels for comparison.

In contrast, M06-2X shows impressively good results already with the moderate 6-31+g(d) basis set (Fig. ESI2, *C*). It is also noteworthy that neither the basis set variation nor the inclusion of the empirical dispersion correction does appreciably alter the optimized geometry. Aiming at higher computational efficiency without using too moderate basis sets, we preferred the slightly smaller triple-zeta basis set 6-311++g(d,p) to the heavier double-zeta aug-cc-pVDZ as the main basis set for our calculations.

A general comparison between the best representatives of each of the two families, *i.e.*, M06-2X and B3LYP-D3 along with the reference results obtained with MP2 and B3LYP is presented in Fig. ESI2D. It is apparent, that even though B3LYP-D3 significantly corrects the main erroneous features of the B3LYP structure, it still performs slightly worse than the M06-2X functional. The latter was thus selected for our main calculations.

Quantitative comparison of the structures presented in Fig. ESI2A is given in Table ESI1. It is evident that the main differences are observed in the ion pairs, *i.e.*, in the relative arrangement of the counterions, but not for the ions themselves. One can also see from Table ESI1 that in the tilted structures obtained with the B3LYP, B97D, and wB97xD functionals the anion is shifted towards the in-plane configuration, as can be judged from the higher values of the $C^4N^3C^2B$ dihedral angle, *i.e.*, the angle between the C^2-B vector and the imidazolium ring plane (the value of 180 degrees would correspond to the perfect in-plane arrangement of the anion, while for anion located exactly above the C^2 carbon a value of 90 degrees is expected). In these structures the anion is also further apart from the center of positive charge of the cation: note the higher values of the $C^2\cdots B$ distances. The latter observation is consistently reflected in reduced values of the interaction energy which is dominated by the Coulomb attraction.[10, 11]

Basic QTAIM properties of the model ion pair $MmimBF_4$ calculated for the structures presented in Fig. ESI2D are collected in Table ESI2. As it was mentioned above for the structural properties, large differences are observed for the ion pairs rather than for the isolated counterions. Since the electron density distribution is determined by the underlying molecular geometry, the differences in the geometries are also reflected in the parameters of the interionic BCPs and in the atomic charges of the relevant atomic sites.

We note that, indeed, as it was anticipated from the geometry of the ion pair, QTAIM analysis reveals several types of weak non-covalent interactions between the counterions, including hydrogen bond like ones (Fig. ESI3). They have intermediate values of the electron density at the BCPs ρ^{BCP} (0.010-0.013 a.u.) and should be classified as weak and electrostatic, since the corresponding values of the Laplacian $\Delta\rho^{BCP}$ and of the total electron energy density H^{BCP} are slightly positive.[12-14] In all the structures discussed here there is a particular BCP and the related bond path connecting the C^2 carbon atom and one of the fluorine atoms of the anion. The corresponding $\rho^{BCP}(C^2\cdots F^1)$ value is comparable with the other hydrogen bond like interionic interactions in this ion pair. A similar BCP was also observed in one of the ion pair structures of BmimCl[15] and in a dimer structure of a set of $Mmim^+$-based ILs.[12, 16, 17] Hunt and co-workers[12, 16, 17] attributed this kind of BCP to so-called anion$\cdots\pi^+$ interaction between an electronegative atom of the anion and the delocalized π-system of the imidazolium cation.

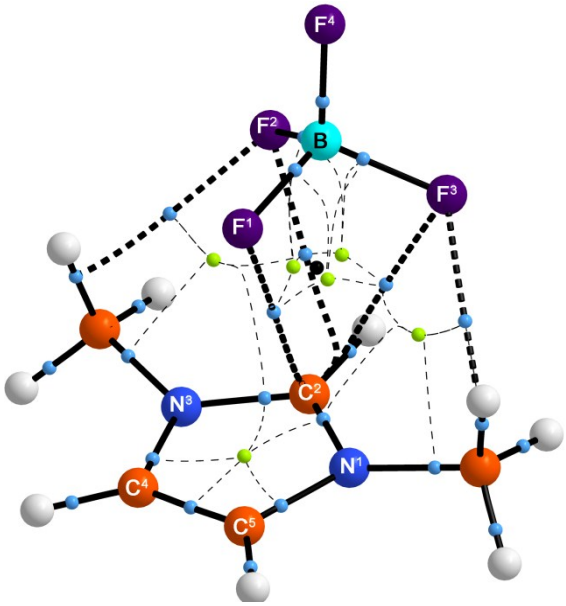

Fig. ESI3. Molecular graph of the MmimBF$_4$ ion pair obtained by means QTAIM analysis of its optimal structure at the MP2/6-311++g(d,p) level of theory. Cage critical point (CCP) is shown as a black sphere, BCPs are light-blue, and ring critical points (RCPs) are green. Bond paths for covalent interactions are shown as solid thick black lines, those of the weak non-covalent ones are thick dashed black lines. Thin dashed black lines show the RCP-to-BCP paths. Color coding of the elements: white – H, orange – C, blue – N, purple – F, cyan – B.

Another prominent feature to mention is that the arrangement of the anion roughly on-top of the C^2-H^2 fragment is not really favorable for directional hydrogen bonding. As a result, the numerical QTAIM algorithm sometimes reveals the corresponding bond paths terminating not at the hydrogen atoms but at the adjacent carbon atoms. The visual inspection of the molecular graph shown in Fig. ESI3 indicates that the bond paths are substantially curved (for example, see the bond paths $F^{3\text{-}2}\cdots C^2$ curving when approaching the carbon site). This is confirmed by rather high values of ellipticity[18], ε^{BCP}, that is a measure of deviation from cylindrical symmetry of electron density distribution (see Table ESI2).

From Fig. ESI3 it is also apparent that within the interionic space in addition to the BCPs there is a number of ring and cage critical points (RCPs and CCPs, respectively). A ring CP is a point of minimum electron density within a quasi-planar ring of interacting atoms and at the same time it is a maximum of ρ along the normal to the ring plane, while a cage CP is a local minimum of ρ in all the directions. It was noted before for weakly bound intermolecular complexes including those with hydrogen bonding that such bonding patterns are indicative of multiple nondirectional non-covalent contacts and the corresponding electron density values, ρ^{RCP} and ρ^{CCP}, can be related to the interaction energies.[19-22] This is in accordance with the recent results of Matthews *et al*. for a set of ion pairs of $Mmim^+$ with different multiatomic anions.[16] As can be seen from Table ESI2, the

ρ^{RCP} and ρ^{CCP} are slightly lower than at the corresponding ρ^{BCP} (ca. 0.008-0.011 a.u.). This proves that there are multiple weak non-covalent interactions in the model $MmimBF_4$ ion pair.

The results of the NCI analysis of the model ion pair are presented in Fig. ESI4. Equation 1 shows that at nuclear sites, where the electron density is high, the gradient reaches zero value leading to low values of the RDG at high ρ values (this region is beyond the bottom right edge of the panel a of Fig. ESI4). At infinite separation from the nuclei, the electron density vanishes and this corresponds to the region of high RDG values as $\rho \rightarrow 0$ (beyond the top left edge of the panel a of Figure. 4). The decay of electron density between these two limiting cases is roughly exponential. As a result, the main trend in the dependence of the RDG on the electron density value is of a general form $\rho^{-1/3}$.[23] However, as it is implied in QTAIM, the bonding pattern in a molecular structure is determined by a set of CPs where the electron density gradient is zero. The BCPs for covalent bonds appear as troughs of zero RDG value at the electron density values corresponding to ρ^{BCP}. For systems with weak non-covalent interactions, whether hydrogen bonding, dispersion or steric repulsion, the corresponding plots reveal similar troughs, but at much lower values of the electron density (typically, below 0.05 a.u.).

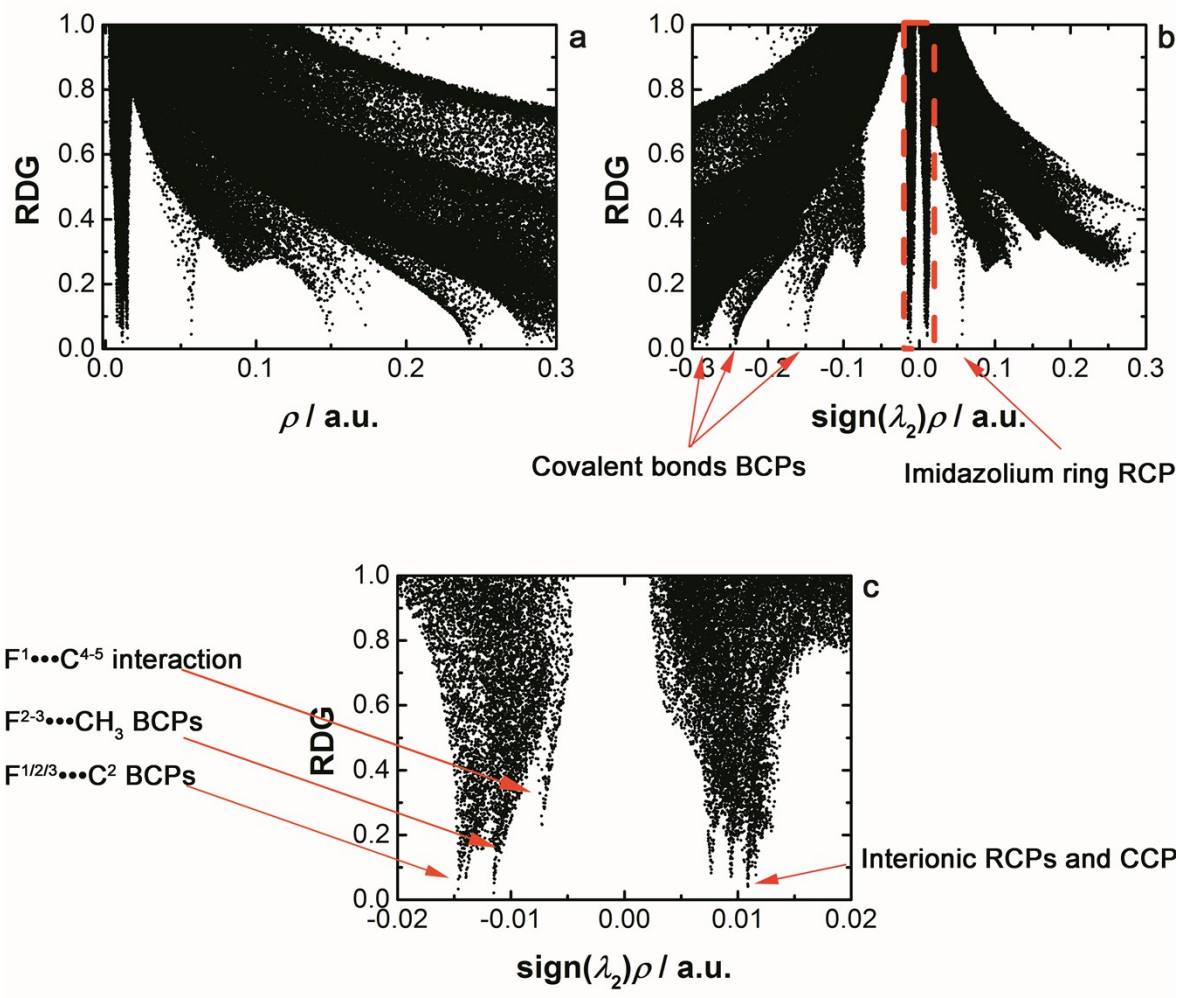

Fig. ESI4. Reduced density gradient as a function of the electron density in $MmimBF_4$ ion pair structure, which was obtained at the MP2/6-311++g(d,p) level of theory (*a*). Reduced density gradient of the same system as a function of the electron density multiplied by the sign of the second eigenvalue of the electron density Hessian (*b*) – NCI plot. Enlarged portion of the NCI plot marked in red, which corresponds to the region of weak non-covalent interactions, is shown in (*c*).

As it was mentioned before, it happens that the electron density gradient itself does not reach zero value for the weak non-covalent interactions, however, the characteristic trough-like pattern is still observed.[24] It reflects the electron density distribution in the vicinity of the anticipated density CP. To distinguish between the attractive and repulsive interactions, it was proposed to use the sign of the second eigenvalue of the electron density Hessian λ_2.[23] For the case of two interacting atoms, the highest eigenvalue λ_3 is positive at the BCP, since it is a minimum of the electron density along the bond path. The λ_2 value characterizes the curvature of the electron density in the plane which is orthogonal to the bond path. For bonding interactions where the electron density is accumulated in the vicinity of the BCP, the λ_2 value is negative, while for the nonbonding and repulsive interactions it is positive. The corresponding graphical representation, often called as NCI plots, is a graph of the RDG plotted as a function of sign(λ_2)ρ, which is shown in the panel b of Fig. ESI4. The covalent bonds, characterized by spikes reaching zero at rather high

values of ρ, appear at the left (negative) side of the NCI plot. The RCP which corresponds to the imidazolium ring gives a spike at the positive side of the NCI plot for $MmimBF_4$ ion pair at *ca*. 0.05 a.u. which perfectly corresponds with the results of QTAIM analysis (Table ESI2).

The region of weak non-covalent interactions between the counterions, which constitutes the main point of interest for us in the present study, is shown in the panel c of Fig. ESI4. The troughs reaching zero RDG values at the negative side of the NCI plot at around *ca*. 0.012-0.015 a.u. correspond to the interionic BCPs revealed by the QTAIM analysis (Table ESI2). Similarly, the troughs at the positive side of the NCI plot in this region correspond to the interionic CCP and RCPs with ρ values of about 0.01 a.u.

A trough at the negative side of the NCI plot which does not reach zero RDG value is an example of a bonding, *i.e.*, stabilizing weak non-covalent interaction which is not captured by the QTAIM analysis. In order to assign this interaction a visualization method is required. Within the NCI approach, this is performed by plotting an isosurface of the RDG which encloses the regions of space where the RDG values are below a given isovalue.[23, 25] The strength of interaction in the regions of non-covalent interactions highlighted by the isosurfaces can be visualized by coloring the surfaces in accordance with the corresponding $\text{sign}(\lambda_2)\rho$ values. A conventional palette for this color mapping of NCI is blue-green-red,[23, 25] that is the regions of bonding interactions with $\text{sign}(\lambda_2)\rho < 0$ are in blue, repulsive interactions and steric clashes where $\text{sign}(\lambda_2)\rho > 0$ are in red, and the weak dispersive interactions of low electron density appear as green isosurfaces. The latter type of interactions is characterized by the electron density values below *ca.* 0.01 a.u. However, despite sufficiently low values of ρ, they are usually rather delocalized and can significantly contribute to the overall pattern of noncovalent interactions.[26, 27]

The NCI isosurfaces for the model $MmimBF_4$ ion pair are shown in Fig. ESI5 along with the non-covalent BCPs, RCPs and the CCP revealed by the QTAIM analysis. One can see an illustrated connection between the results of QTAIM and NCI analyses. The BCPs are located in the center of blueish regions of the NCI isosurfaces, the RCPs and the CCP in the region between the counterions correspond to green-yellow parts of the surfaces (weak van der Waals interactions). The imidazolium ring RCP is in between the two distinctly red colored NCI regions which is indicative of destabilizing crowding of the electron density due to the ring closure. The red traces around the B-F bonds in the anion are due to steric clashes between the electron shells of the electron-rich fluorine atoms.

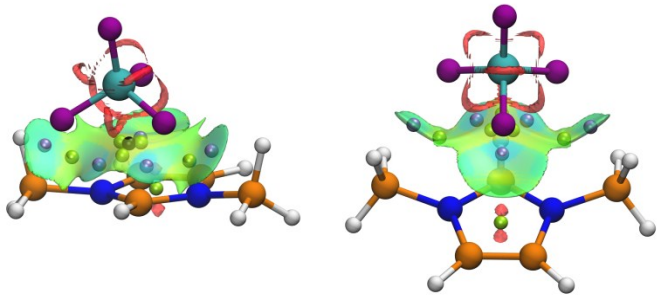

Fig. ESI5. NCI isosurfaces for the $MmimBF_4$ ion pair structure, which was obtained at the MP2/6-311++g(d,p) level of theory. The reduced density gradient cut-off value is 0.6. The sign(λ_2)ρ value is colormapped onto the isosurfaces in the region from −0.03 a.u. to +0.03 a.u. in the blue-green-red palette. CPs revealed by the QTAIM analysis are shown for comparison: BCPs as light blue spheres, RCPs as green spheres, and CCP is shown in black. Color coding of the elements: white – H, orange – C, blue – N, purple – F, cyan – B. The two images represent different points of view.

The only blueish-green part of the NCI isosurface in the space between the counterions, that does not contain a BCP, is the one between the F^1 atom and the $C^{4\text{-}5}$ site. This corresponds to the feature noted in the NCI plot (Fig. ESI4) as a spike at low negative sign(λ_2)ρ values that does not reach zero RDG values.

From this brief analysis of the electron density distribution in the model ion pair $MmimBF_4$, it is apparent that due to the multiatomic nature of the counterions a broad and delocalized surface of weak non-covalent interactions is established in the interionic space. Their relative strength between selected fragments can be estimated via the NCI surfaces and plots. The results are not only compatible with the QTAIM analysis of CPs, but can also reveal stabilizing interactions which cannot be captured within the QTAIM approach.

In order to assess the influence of the level of theory on the results of NCI analysis, as it was done for QTAIM in the previous section the NCI plots for the model ion pair obtained with different methods and the 6-311++g(d,p) basis set are compared in Fig. ESI6.

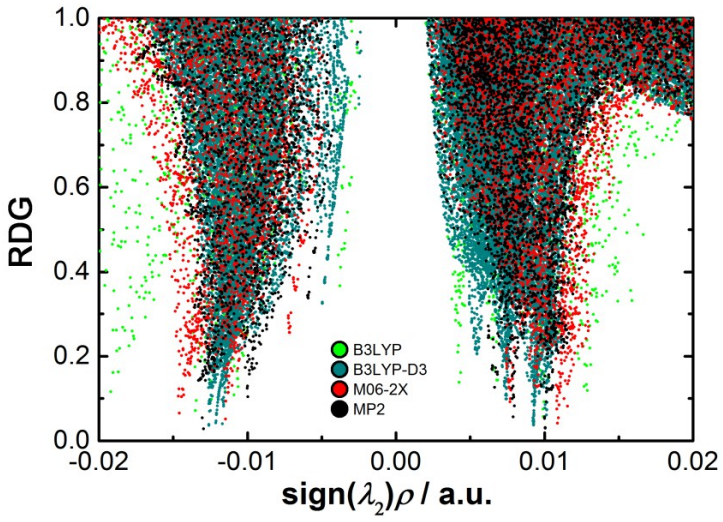

Fig. ESI6. NCI plot for the $MmimBF_4$ ion pair structures which were obtained with different methods coupled with the 6-311++g(d,p) basis set.

Similarly to structural and QTAIM analyses, B3LYP is an outlier due to too poor geometry. M06-2X, which was selected as the working functional for the present study, slightly overestimates the electron densities in the region of bonded interactions, but performs well in the region of weak repulsive and van der Waals interactions, when referenced to MP2.

Table ESI1. Comparison of the main geometrical and energetic properties for $MmimBF_4$ ion pair and its isolated ions calculated at different levels of theory in vacuum.

	B3LYP/6-31+g(d)	**B3LYP/6-311++g(d,p)**	**B3LYP-D3/6-311++g(d,p)**	**B97D/6-311++g(d,p)**	**wB97xD/6-311++g(d,p)**	**M06-2X/6-31+g(d)**	**M06-2X/6-311++g(d,p)**	**M06-2X-D3/6-311++g(d,p)**	**M06-2X/aug-cc-pVDZ**	**MP2/6-311++g(d,p)**	**MP2/aug-cc-pVTZ**
BF_4^-											
d(B-F) / Å	1.418	1.417	1.419	1.432	1.414	1.409	1.409	1.409	1.415	1.415	1.409
$Mmim^+$											
d($C^{4\text{-}5}$-H) / Å	1.080	1.077	1.077	1.081	1.077	1.080	1.077	1.077	1.083	1.080	1.076
d(C^2-H) / Å	1.080	1.078	1.077	1.081	1.078	1.081	1.079	1.079	1.083	1.080	1.076
∠ NC^2N / deg.	108.96	108.86	108.77	108.61	108.89	108.82	108.83	108.84	108.76	108.38	108.31
∠ $HCNC^2$ / deg.	0.00	1.14	1.15	0.05	1.13	0.98	1.24	0.03	0.00	1.23	1.11
$MmimBF_4$											
max *d*(B-F) / Å	1.440	1.439	1.431	1.446	1.431	1.422	1.422	1.422	1.427	1.427	1.422
min *d*(B-F) / Å	1.377	1.374	1.377	1.389	1.374	1.373	1.370	1.370	1.378	1.377	1.374
d($C^{4\text{-}5}$-H) / Å	1.079	1.076	1.076	1.080	1.076	1.079	1.076	1.076	1.081	1.079	1.075
d(C^2-H) / Å	1.082	1.078	1.076	1.079	1.078	1.080	1.077	1.077	1.082	1.077	1.074
∠ NC^2N / deg.	108.81	108.81	108.75	108.58	108.87	108.80	108.84	108.84	108.75	108.42	108.24
∠ $HCN^{1/3}C2$ / deg.	0.84/25.58	7.76/23.92	38.03	36.45/37.73	25.99/32.21	22.11	22.46	22.46	24.23	25.77	21.86
d(C···B) / Å	3.129	3.103	3.018	3.071	3.030	2.926	2.924	2.924	2.908	2.983	2.959
∠ $C^4N^3C^2B$ / deg.	130.46	127.87	104.35	108.88	110.42	101.60	101.71	101.71	103.54	102.28	101.97
$-E^{int}$ / kJ mol^{-1}	347.9	353.8	375.3	369.4	369.2	380.7	387.3	388.7	388.1	376.8	377.7
No of basis functions	246	327	327	327	327	246	327	327	357	327	759

Table ESI2. Comparison of the main QTAIM parameters for $MmimBF_4$ ion pair and its isolated ions calculated at different levels of theory in vacuum.

	B3LYP/6-311++g(d,p)	**B3LYP-D3/6-311++g(d,p)**	**M06-2X/6-311++g(d,p)**	**MP2/6-311++g(d,p)**
BF_4^-				
q(F) / e	−0.839	−0.839	−0.853	−0.856
$Mmim^+$				
$q(C^2)$ / e	0.995	0.995	1.070	0.997
$q(H^2)$ / e	0.149	0.150	0.154	0.159
$MmimBF_4$				
$q(BF_4^-)$ / e	−0.969	−0.977	−0.986	−0.987
$q(C^2)$ / e	1.018	1.029	1.110	1.044
$q(H^2)$ / e	0.231	0.191	0.191	0.195
BCPs				
$\rho^{BCP}(C^2\cdots F^1)$ / a.u.	0.0109	0.0121	0.0140	0.0133
$\Delta\rho^{BCP}(C^2\cdots F^1)$ / a.u.	0.0429	0.0477	0.0569	0.0528
$H^{BCP}(C^2\cdots F^1)$ / a.u.	0.0014	0.0012	0.0011	0.0010
$\varepsilon^{BCP}(C^2\cdots F^1)$	0.77	0.37	0.62	0.42
$\rho^{BCP}(H^2\cdots F^{2\text{-}3})$ / a.u.	0.0136/0.0192	0.0126	-	-
$\Delta\rho^{BCP}(H^2\cdots F^{2\text{-}3})$ / a.u.	0.0744/0.0558	0.0518	-	-
$H^{BCP}(H^2\cdots F^{2\text{-}3})$ / a.u.	0.0021/0.0020	0.0018	-	-
$\varepsilon(H^2\cdots F^{2\text{-}3})$	0.05/0.36	0.43	-	-
$\rho^{BCP}(C^2\cdots F^{2\text{-}3})$ / a.u.	-	-	0.0146	0.0130
$\Delta\rho^{BCP}(C^2\cdots F^{2\text{-}3})$ / a.u.	-	-	0.0609	0.0547
$H^{BCP}(C^2\cdots F^{2\text{-}3})$ / a.u.	-	-	0.0017	0.0016
$\varepsilon^{BCP}(C^2\cdots F^{2\text{-}3})$	-	-	0.65	0.60
$\rho^{BCP}(H^{Me}\cdots F^{2\text{-}3})$ / a.u.	0.0125/0.0115	0.0117	-	0.0102
$\Delta\rho^{BCP}(H^{Me}\cdots F^{2\text{-}3})$ / a.u	0.0461/0.0407	0.0453	-	0.0431
$H^{BCP}(H^{Me}\cdots F^{2\text{-}3})$ / a.u	0.0014/0.012	0.0014	-	0.0010
$\varepsilon^{BCP}(H^{Me}\cdots F^{2\text{-}3})$	0.01/0.07	0.35	-	0.76
$\rho^{BCP}(C^{Me}\cdots F^{2\text{-}3})$ / a.u.	-	-	0.0115	-
$\Delta\rho^{BCP}(C^{Me}\cdots F^{2\text{-}3})$ / a.u.	-	-	0.0500	-
$H^{BCP}(C^{Me}\cdots F^{2\text{-}3})$ / a.u.	-	-	0.0015	-
$\varepsilon^{BCP}(C^{Me}\cdots F^{2\text{-}3})$	-	-	1.02	-
RCPs				
ρ^{RCP} (imidazolium)/ a.u.	0.0545	0.0547	0.0570	0.0551
ρ^{RCP} (interionic)/ a.u.	0.0065-0.0128	0.0074-0.0101	0.0094-0.0116	0.0079-0.0105
CCPs				
ρ^{CCP} / a.u.	-	0.0092	0.0108	0.0100

1. E. I. Izgorodina and D. R. MacFarlane, *J. Phys. Chem. B*, 2011, **115**, 14659-14667.
2. S. Zahn, F. Uhlig, J. Thar, C. Spickermann and B. Kirchner, *Angew. Chem., Int. Ed.*, 2008, **47**, 3639-3641.
3. E. I. Izgorodina, J. Rigby and D. R. MacFarlane, *Chem. Commun.*, 2012, **48**, 1493-1495.
4. E. I. Izgorodina, D. Golze, R. Maganti, V. Armel, M. Taige, T. J. S. Schubert and D. R. MacFarlane, *Phys. Chem. Chem. Phys.*, 2014, **16**, 7209-7221.
5. V. Kempter and B. Kirchner, *J. Mol. Struct.*, 2010, **972**, 22-34.

6. S. Zahn, D. R. MacFarlane and E. I. Izgorodina, *Phys. Chem. Chem. Phys.*, 2013, **15**, 13664-13675.
7. R. P. Matthews, T. Welton and P. A. Hunt, *Phys. Chem. Chem. Phys.*, 2014, **16**, 3238-3253.
8. C. Fong-Padrón, E. M. Cabaleiro-Lago and J. Rodríguez-Otero, *Chem. Phys. Lett.*, 2014, **593**, 181-188.
9. P. A. Hunt, B. Kirchner and T. Welton, *Chem. – Eur. J.*, 2006, **12**, 6762-6775.
10. S. Tsuzuki, H. Tokuda, K. Hayamizu and M. Watanabe, *J. Phys. Chem. B*, 2005, **109**, 16474-16481.
11. S. Tsuzuki, H. Tokuda and M. Mikami, *Phys. Chem. Chem. Phys.*, 2007, **9**, 4780-4784.
12. P. A. Hunt, C. R. Ashworth and R. P. Matthews, *Chem. Soc. Rev.*, 2015, **44**, 1257-1288.
13. S. J. Grabowski, *Chem. Rev.*, 2011, **111**, 2597-2625.
14. U. Koch and P. L. A. Popelier, *J. Phys. Chem.*, 1995, **99**, 9747-9754.
15. L. del Olmo, C. Morera-Boado, R. López and J. García de la Vega, *J. Mol. Model.*, 2014, **20**, 1-10.
16. R. P. Matthews, C. Ashworth, W. Tom and A. H. Patricia, *J. Phys.: Condens. Matter*, 2014, **26**, 284112.
17. R. P. Matthews, T. Welton and P. A. Hunt, *Phys. Chem. Chem. Phys.*, 2015, DOI: 10.1039/C5CP00459D.
18. R. F. W. Bader, *Chem. Rev.*, 1991, **91**, 893-928.
19. S. J. Grabowski and M. Małecka, *J. Phys. Chem. A*, 2006, **110**, 11847-11854.
20. C. Estarellas, A. Frontera, D. Quiñonero and P. M. Deyà, *J. Phys. Chem. A*, 2011, **115**, 7849-7857.
21. D. Vijay and G. N. Sastry, *Chem. Phys. Lett.*, 2010, **485**, 235-242.
22. O. A. Zhikol, O. V. Shishkin, K. A. Lyssenko and J. Leszczynski, *J. Chem. Phys.*, 2005, **122**, 144104.
23. E. R. Johnson, S. Keinan, P. Mori-Sánchez, J. Contreras-García, A. J. Cohen and W. Yang, *J. Am. Chem. Soc.*, 2010, **132**, 6498-6506.
24. J. R. Lane, J. Contreras-García, J.-P. Piquemal, B. J. Miller and H. G. Kjaergaard, *J. Chem. Theory Comput.*, 2013, **9**, 3263-3266.
25. J. Contreras-García, E. R. Johnson, S. Keinan, R. Chaudret, J.-P. Piquemal, D. N. Beratan and W. Yang, *J. Chem. Theory Comput.*, 2011, **7**, 625-632.
26. A. Otero-de-la-Roza, E. R. Johnson and J. Contreras-Garcia, *Phys. Chem. Chem. Phys.*, 2012, **14**, 12165-12172.
27. R. Chaudret, B. de Courcy, J. Contreras-Garcia, E. Gloaguen, A. Zehnacker-Rentien, M. Mons and J. P. Piquemal, *Phys. Chem. Chem. Phys.*, 2014, **16**, 9876-9891.